FRAGMENTATION OF SHELL-LIKE SYSTEMS

Falk K. Wittel[1], Ferenc Kun[2], Hans J. Herrmann[3], and Bernd H. Kröplin[1]

[1]Institute for Statics and Dynamics of Aerospace Structures, University of Stuttgart, Pfaffenwaldring 27, 70569 Stuttgart, Germany
[2]Department of Theoretical Physics, University of Debrecen, P. O. Box: 5, H-4010 Debrecen, Hungary
[3]Institute for Computer Physics, University of Stuttgart, Pfaffenwaldring 27, D-70569 Stuttgart, Germany

ABSTRACT

A detailed study of the fragmentation of closed thin shells made of a disordered brittle material is presented. For the theoretical investigations a three dimensional discrete element model of shells is constructed. Molecular dynamics simulations of two extreme loading cases resulted in power law fragment mass distributions showing satisfactory agreement with experiments on egg-shells, hollow plastic and glass spheres. Two different loading conditions are studied: fragmentation due to an impact with a hard wall and explosion by a combustion mixture. Based on large scale simulations we give evidence that power law distributions arise due to an underlying phase transition which proved to be abrupt and continuous for explosion and impact, respectively. Our results demonstrate that the fragmentation of closed shells defines a universality class different from that of two and three dimensional bulk systems.

1. INTRODUCTION

Explosive fragmentation of rocket stages and satellites due to self-ignition are one of the main sources of space debris that orbits earth, witnessing more than 4 decades of space activity. Fragmentation, in other words the breaking of particulate material into numerous smaller pieces is a universal phenomenon and can be observed on a wide range of length scales in all kinds of technical applications and nature as well. The number of fragments larger 1mm that orbit earth at speeds of up to 10km/s can only be estimated to be larger $3 \cdot 10^6$, but their destructive potential for operational satellites and manned space flight is enormous due to their kinetic energy. Since only fragments larger 5mm can be detected and cataloged from radar stations on earth, the largest number of fragments remains unwatched Oswald et al. (2004). Therefore knowledge about their initial formation - the fragmentation process - becomes important for numeric predictions on the positions of the fragment population. From the structural point of view, aircrafts, containers, launch vehicles like rockets or building blocks of space stations are shell-like systems. Most studies focus on the behavior of bulk systems in one, two and tree dimensions under impact and explosive loading, showing universal power law behavior of fragment size distribution, however, hardly any studies have been devoted to fragmentation of shells.

We study fragmentation of closed thin shells made of disordered brittle material due to an excess load inside the system. Owing to the complexity of the damage process during fragmentation, analytic descriptions are strongly limited. However, numeric simulations like molecular dynamic simulations with discrete element models the simultaneous initiation and dynamic propagation of a large amount of interacting cracks can be considered. Based on large-scale simulations with spherical shell systems under different extreme loading situations, we prove a power law for the fragment mass distribution and give evidence that it arises due to an underlying phase transition. The system can be interpreted as a spherical rocket tank that behaves brittle due to its temperature. Emphasis is given on scaling relations for fragment masses. The peculiarity of the fragmentation of shell systems from two- and three-dimensional objects originates from the fact, that the local structure is inherently two-dimensional, the dynamics of the systems however is three-dimensional which allows for a rich variety of failure modes. The theoretical study is supported by experiments performed on hen egg-shells, as well as on thin walled plastic and glass spheres, fragmented due to an impact with a hard wall and explosion by a combustion mixture inside the shell. Satisfactory agreement is found between the numerical predictions of the exponent of the power law for the fragment mass distribution and the experimental findings.

Proceedings of the Fourth European Conference on Space Debris, Darmstadt, Germany, 18-20 April 2005
(ESA SP-587, August 2005)

2. SIMULATION OF THE BREAK-UP PROCESS

Theoretical studies on fragmentation often relay on large scale computer simulations. Capabilities of analytic approaches to fragmentation are rather limited due to the complexity of the break-up process. Over the past years Discrete Element Methods (DEM) proved to be a very efficient numerical tool for fracture and fragmentation phenomena Åström et al. (1997, 2000); Kun & Herrmann (1999); Wittel et al. (2004); Potapov et al. (1995) since it has the ability to handle large deformations arising dynamically, and naturally captures the propagation and interaction of a large number of simultaneously growing cracks, which is essential for fragmentation.

We constructed a three-dimensional discrete element model to investigate the fragmentation of spherical shells, such that the surface of the unit sphere is discretized into randomly shaped triangles by throwing points randomly and independently on the surface with a minimum distance to neighboring points. Based on the Delaunay triangulation, the dual Voronoi tessellation of the surface is carried out. The nodes of the triangulation represent point-like material elements in the model whose mass is defined by the area of the Voronoi polygon assigned to it. The elements between nodes are assumed to be springs with linear elastic behavior up to failure. Disorder is introduced in the model solely by the randomness of the tessellation so that the mass assigned to the nodes, furthermore, the length and cross-section of the springs are determined by the tessellation. After prescribing the initial conditions of a specific fragmentation process studied, the time evolution of the system is followed by solving the equation of motion of nodes by a Predictor-Corrector method, namely

$$m_i\ddot{\vec{r}}_i = \vec{F}_i^s + \vec{F}_i^{ext} + \vec{F}_i^d, \quad i = 1, \dots N, \tag{1}$$

where $\vec{F}_i^s$ is the sum of forces exerted by the elements connected to node i, and $\vec{F}_i^{ext}$ denotes the external driving force, which depends on the loading condition and $\vec{F}_i^d$ is a small viscous damping force.

In order to account for damage, the elements are assumed to break when their deformation ε exceeds a fixed breaking threshold ε_c, resulting in a random sequence of breakings due to the disordered element properties. The breaking criterion is evaluated in each iteration step and those elements which fulfill the condition are removed from the simulation. As a result of successive element breakings, cracks nucleate, propagate, bifurcate and merge on the spherical surface which can give rise to a complete fragmentation of the shell into smaller pieces.

Fragments of the shell are defined in the model as sets of nodes (material elements) connected by the

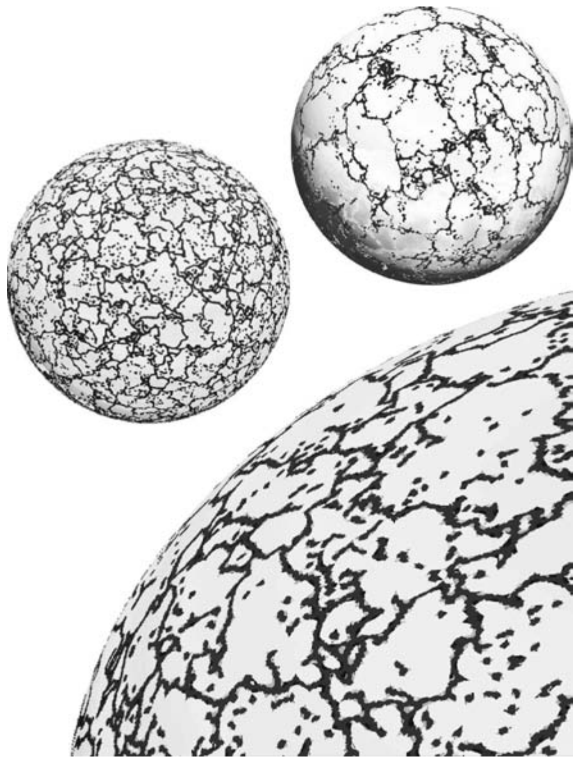

Figure 1. Cracks on the shell surface for impact (left and closeup) and pressure (right) loading, projected to the initial position.

remaining intact elements. The process is stopped when the system has attained a relaxed state, *i.e.* when there is no element breaking over a longer time interval. The main advantage of DEM is that it makes possible to monitor a large number of microscopic physical quantities during the course of the simulation which are hardly accessible experimentally, providing a deep insight into the fragmentation process. At the present computer capacities, DEM models can be designed to be realistic so that the simulation results can even complement the experimental information extending our understanding.

In our computer simulations two different ways of loading have been considered which model the experimental conditions and represent limiting cases of energy input rates: *(i)* pressure pulse and *(ii)* impact load. A pressure pulse is carried out by imposing a fixed internal pressure P_o from which the forces $\vec{F}_j^{ext}$ acting on the triangular surface elements are calculated as $\vec{F}_j^{ext} = P_o A_j \vec{n}_j$, where A_j denotes the actual area of triangle j and the force points in the direction of the local normal $\vec{n}_j$. The force F_j^{ext} is equally shared by the three nodes of the triangle for which the equation of motion (Eq. 1) is solved. Since the surface area of the shell increases, the expansion under constant pressure implies a continuous increase of the driving force and of the imparted energy.

The impact loading realizes the limiting case of instantaneous energy input by giving initial velocity v_o to the material elements pointing radially outward and following the resulted time evolution of the system by solving the equation of motion Eq. (1). The control parameter of the system which determines the final outcome of the process is the fixed pressure P_o and the initial kinetic energy E_o for the pressure pulse and impact loading, respectively.

3. SCALING RELATIONS FOR FRAGMENTATION PREDICTIONS

To characterize the break-up of shells quantitatively and to reveal the nature of the transition between the damaged and fragmented states, large scale simulations have been performed with broadly varying control parameters P_o and E_o. The most important characteristic of our fragmenting shell system is the variation of fragment masses when changing the control parameters. Numerically found scaling relations are the key for understanding fragmentation processes. If scaling is not understood, a theory itself is not understood. In the simulations two cutoffs for the fragment masses arise, with the lower one being defined by the single unbreakable material elements of the model and the upper one originating from the finite size of the system.

3.1. Largest Fragments

The size of the largest fragment is not only interesting for space application, *e.g.* thinking of reentry of fragment, but it is also a important property to characterize the degree of fragmentation, *i.e.* the size reduction achieved in the simulations. We calculated the average mass of the largest $\langle M_{max}/M_{tot}\rangle$ and of the second largest $\langle M_{max}^{2nd}/M_{tot}\rangle$ fragment normalized by the total mass as a function of P_o and E_o in the case of pressure and impact loading, respectively Kun & Herrmann (1999). The results are presented in Fig. 2. It can be seen that in both loading cases the maximum fragment mass is a monotonically decreasing function of the control parameters P_o and E_o, however, the functional forms are different in the two cases. Low pressure values in Fig. 2A result in a breaking of elements, however, hardly any fragments are formed except for single elements broken out of the shell along cracks. The value of the critical pressure P_c needed to achieve fragmentation and the functional form of the curve of $\langle M_{max}/M_{tot}\rangle$ above P_c was determined such that $\langle M_{max}/M_{tot}\rangle$ was plotted as a function of the difference $|P_o - P_c|$ varying P_c until a straight line is obtained on a double logarithmic plot (see inset of Fig. 2A), where a power law dependence of $\langle M_{max}/M_{tot}\rangle$ is evidenced on the distance from the critical point

$$\langle M_{max}/M_{tot}\rangle \sim |P_o - P_c|^{-\alpha}, \quad \text{for} \quad P_o > P_c. \tag{2}$$

For the value of the exponent $\alpha = 0.66 \pm 0.02$ was obtained, showing good agreement with analytic predictions (see Wittel et al. (2004)). Detailed studies in the vicinity of P_c revealed a finite jump of both $\langle M_{max}/M_{tot}\rangle$ and $\langle M_{max}^{2nd}/M_{tot}\rangle$ at P_c which implies that fragmentation occurs as an abrupt transition at the critical point.

In Fig. 2B the corresponding results are presented for the case of impact loading as a function of the total energy E_o imparted to the system. Careful analyzes revealed the existence of two regimes with a continuous transition at a critical value of the imparted energy E_c. In the inset of Fig. 2B $\langle M_{max}/M_{tot}\rangle$ is shown as a function of the distance from the critical point $|E_o - E_c|$ where E_c was determined with the same technique as P_c. Contrary to the pressure loading, $\langle M_{max}/M_{tot}\rangle$ exhibits a power law behavior on both sides of the critical point though having different exponents

$$\langle M_{max}/M_{tot}\rangle \sim |E_o - E_c|^{\beta}, \quad \text{for} \quad E_o < E_c \tag{3}$$

$$\langle M_{max}/M_{tot}\rangle \sim |E_o - E_c|^{-\alpha}, \quad \text{for} \quad E_o > E_c \tag{4}$$

The numerical values of the exponents were obtained as $\alpha = 0.66 \pm 0.02$ and $\beta = 0.5 \pm 0.02$, above and below the critical point respectively. Note that α coincides with α of the pressure loading.

3.2. Average Fragment Mass

More insight into the fragmentation process can be obtained by studying the so-called single event moments of fragment masses

$$M_k^j = \sum_m m^k n^j(m) - M_{max}^k, \tag{5}$$

where M_k^j denotes the k-th moments of fragment masses m in the jth realization of the fragmentation process, $n^j(m)$ is the number of fragments of mass m in event j. The ratio $M^j = M_2^j/M_1^j$ of the second M_2^j and the first M_1^j moments provides a measure of the average fragment mass in a specific experiment j. Averaging over simulations with different realizations of disorder the average fragment mass $\overline{M} = < M_2^j/M_1^j >$ was obtained as a function of the control parameters of the system.

Due to the abrupt nature of the transition from the damaged to the fragmented states at the critical pressure, under pressure loading $\overline{M}$ cannot be evaluated below P_c. However, when P_o exceeds the critical pressure P_c the average fragment mass monotonically decreases in Fig. 2C. The inset of Fig. 2C shows $\overline{M}$ as a function of the distance from the critical point $|P_o - P_c|$ where the same value of P_c was used as in Fig. 2A. A power law dependence of $\overline{M}$ is evidenced on $|P_o - P_c|$

$$\overline{M} \sim |P_o - P_c|^{-\gamma}, \tag{6}$$

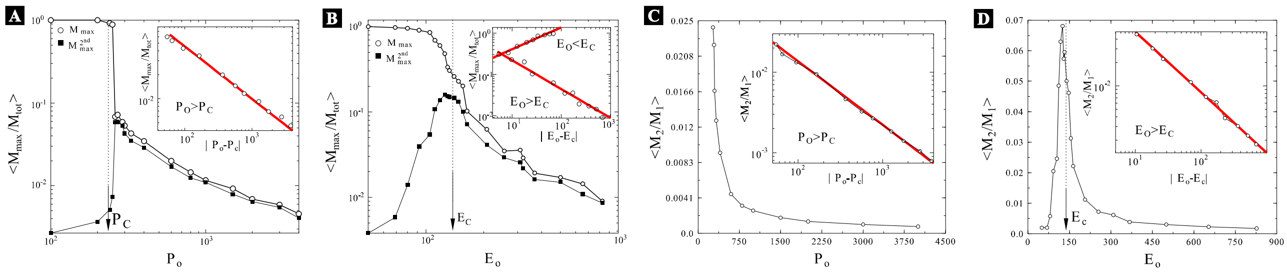

Figure 2. Average mass of the largest $\langle M_{max}/M_{tot}\rangle$ and second largest $\langle M^{2nd}_{max}/M_{tot}\rangle$ fragment normalized by the total mass as a function of imposed pressure P_o and impact energy E_o (A,B). C,D shows the average fragment mass as a function of the imposed pressure P_o and impact energy E_o. The insets present the results as a function of the distance from the critical point $P_o - P_c$ for $P_o > P_c$ and $E_o - E_c$ for energy values $E_o > E_c$.

for $P_o > P_c$ and the value of the exponent was obtained to be $\gamma = 0.8 \pm 0.02$. For impact loading $\overline{M}$ can be evaluated on both sides of the critical point with a sharp peak in the vicinity of E_c which is typical for continuous phase transitions in finite systems, see Fig. 2D. A power law dependence of $\overline{M}$ on the distance from the critical point

$$\overline{M} \sim |E_o - E_c|^{-\gamma} \tag{7}$$

is revealed again for $E_o > E_c$ (see inset of Fig. 2D). The value of the exponent was determined by fitting $\gamma = 0.79 \pm 0.02$, which practically coincides with the γ value of pressure loading.

3.3. Fragment Mass Distribution

The most important characteristic quantity for the formation of space debris is the mass distribution of fragment cloud $F(m)$. For impact loading for $E_o < E_c$ we found that $F(m)$ has a pronounced peak at large fragments indicating the presence of large damaged pieces, see Fig. 3A. Approaching the critical point E_c the peak gradually disappears and the distribution asymptotically becomes a power law at E_c. It can be observed in Fig. 3A that above the critical point the power law remains valid for small fragments followed by a cut-off for the large ones, which decreases with increasing E_o.

For pressure loading $F(m)$ can only be evaluated above P_c. The evolution of $F(m)$ with increasing pressure is presented in Fig. 3B, where the mass distribution always shows a power law behavior for small fragments with a relatively broad cut-off for the large ones. For the purpose of comparison, a mass distribution $F(m)$ obtained at an impact energy close to the critical point E_c, and distributions at two different pressure values P_o of the ratio 1.6 are plotted in Fig. 5 along with the experimental results.

Fig. 3C,D demonstrate that by rescaling the mass distributions above the critical point by plotting $F(m) \cdot \overline{M}^{\delta}$ as a function of $m/\overline{M}$ an excellent data collapse is obtained with $\delta = 1.6 \pm 0.03$. The data collapse implies the validity of the scaling form

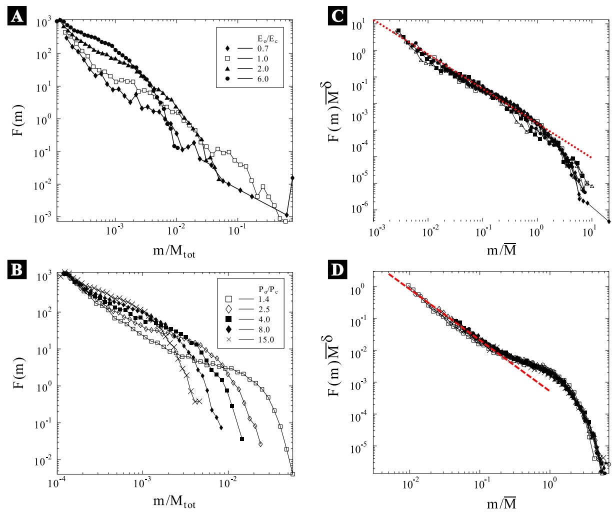

Figure 3. Mass distribution of fragments at various energies (A) and pressures (B) below and above the critical point. Rescaled plot of the mass distributions for imparted energies above the critical points $E_o > E_c$ (C) and $P_o > P_c$ (D). The dashed line shows the fitted power law of an exponent 1.35 ± 0.03.

$$F(m) \sim m^{-\tau} \cdot f(m/\overline{M}), \tag{8}$$

typical for critical phenomena. The cut-off function f has a simple exponential form $exp(-m/\overline{M})$ for impact loading (see Fig. 3C), and a more complex one containing also an exponential component for the pressure case (see Fig. 3D). The average fragment mass $\overline{M}$ occurring in the scaling form Eq. (8) diverges according to a power law Eqs. (6,7) when approaching the critical point. The good quality of collapse and the functional form Eq. (8) also imply that the exponent τ of the mass distribution does not depend on the value of the pressure P_o or the kinetic energy E_o contrary to the bulk fragmentation where an energy dependence of τ was reported.

The rescaled plots render an accurate determination of the exponent τ possible, where $\tau = 1.35 \pm 0.03$ and $\tau = 1.55 \pm 0.03$ were obtained for impact and pressure loading, respectively. This scaling relation might help to overcome the gap between low- and high-intensity explosion events described in Klinkrad et al. (2001).

4. EXPERIMENTS ON FRAGMENTATION

Published experiments on shell fragmentation are very limited. We found that the simples way to experiment with shell fragmentation is to utilize hen egg shells. Hen eggs provide an excellent possibility for the study of fragmentation of thin brittle shells of disordered materials with the additional advantages of being cheap and easy to handle. In the preparations, first two holes of regular circular shape were drilled on the bottom and top of the egg through which the content of the egg was blown-out. The inside was carefully washed and rinsed and finally the empty shells were dried. Explosion experiments were also performed on hollow glass spheres. In the impact experiments intact egg shells, glass and nitrogen cooled plastic spheres are catapulted onto the ground at a high speed using a simple setup of rubber bands.

In the explosion experiments the objects are flooded with a stoichiometric hydrogen/oxygen mixture and hung inside a plastic bag. The combustion reaction is initiated by a spark in the center of the object. The reaction is carried out inside a soft plastic bag so that secondary fragmentation due to fragment-wall collisions does not occur, furthermore, no pieces were lost after explosion. Since the pressure which builds up during combustion can slightly be controlled by the hole size, *i.e* the smaller the hole is, the higher the pressure at the explosion is, we performed several series of experiments with hole diameters d between 1.2 and 2.5mm.

It is possible to follow the time evolution of the explosion and impact processes by means of a high speed camera (see Fig. 4). In the damage evolution fragment formation by crack bifurcation and coalescence can be evidenced for both materials. Note that glass is an amorphous material with deviation crack growth mechanisms than brittle disordered materials, *e.g.* hot spots for crack nucleation can be observed. Based on the snapshots the total duration of an explosion is estimated to be of the order of 0.3ms.

After the breaking, fragments are carefully placed on the tray of a scanner without overlap. In the scanned image fragments occur as, for instance, black spots on a white background (see Fig. 5) and were further analyzed by a cluster searching code. A dusty phase of shattered pieces Redner (1990) was also observed in the experiments with fragment sizes falling in the order of the pixel size of the scanner. The mass m of fragments was determined as the number of pixels of spots in the scanned image.

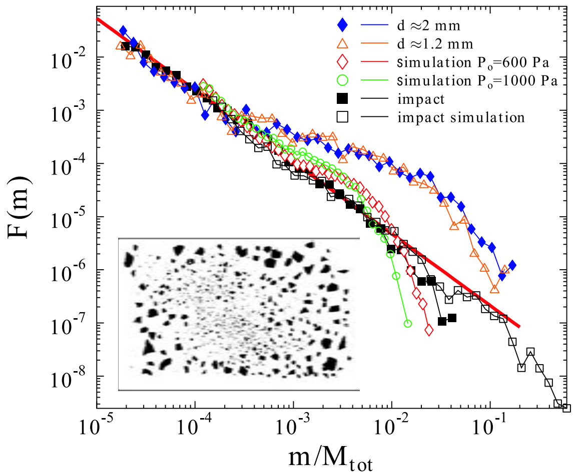

Figure 5. Comparison of fragment mass distributions obtained by explosion experiments with two hole sizes and in the impact experiment to the simulation results.

As the main quantitative result of the experiments we evaluated the mass distribution of fragments $F(m)$ which is defined so that $F(m)\Delta m$ provides the probability of finding a fragment with mass value falling between m and $m + \Delta m$. Fig. 5 presents the fragment mass distributions $F(m)$ for impact and explosion experiments averaged over 10-20 egg-shells for each curve. For the impact experiment, a power law behavior of the fragment mass distribution

$$F(m) \sim m^{-\tau} \tag{9}$$

can be observed over three orders of magnitude where the value of the exponent can be determined with high precision to $\tau = 1.35 \pm 0.02$. Explosion experiments result also in a power law distribution of the same value of τ for small fragments with a relatively broad cut-off for the large ones. Smaller hole diameter d in Fig. 5, *i.e.* higher pressure, gives rise to a larger number of fragments with a smaller cut-off mass and a faster decay of the distribution $F(m)$ at the large fragments. Note that the relatively small value of the exponent τ can indicate a cleavage mechanism of shell fragmentation and is significantly different from the experimental and theoretical results on fragmenting two-dimensional bulk systems where $1.5 \leq \tau \leq 2$ has been found Turcotte (1986); Inaoka et al. (1997); Kadono (1997); Åström et al. (1997); Kun & Herrmann (1999), and from the three-dimensional ones where $\tau > 2$ is obtained Turcotte (1986); Fujiwara & Tsukamoto (1980); Thornton et al. (1996); Benz & Asphaug (1994). Hence, a good quantitative agreement of the theoretical and experimental values of the exponent τ is evidenced for the impact loading of shells. However, for the case of pressure loading the numerically

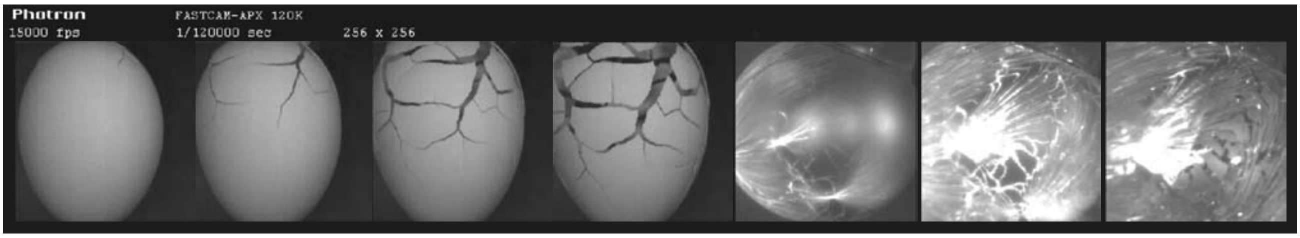

Figure 4. Time evolution of the explosion of an egg and a hollow glass sphere. Consecutive snapshots taken by a high speed camera at 15kHz.

obtained exponent turned out to be higher than in the case of exploded eggs.

5. DISCUSSION AND OUTLOOK

We presented a detailed experimental and theoretical study of the break-up of closed shells arising due to a shock inside the shell. We worked out a discrete element model of the break-up of shells which provides a deep insight into the dynamics of the process by simultaneously monitoring several microscopic quantities in the framework of molecular dynamics simulations. In the simulations two ways of loading have been considered, which mimic the experimental conditions and represent limiting cases of energy input rates: during an expansion under constant pressure P_o the shell is driven by an increasing force with a continuous increase of the imparted energy, while the impact loading realizes the instantaneous input of the energy E_o. Simulations revealed that depending on the value of P_o and E_o, the final outcome of the break-up process can be classified into two states, *i.e.* damaged and fragmented states with a sharp transition in between at a critical value of the control parameters P_c and E_c. In the fragmented regime power law fragment mass distributions were obtained in a satisfactory agreement with the experimental findings. Analyzing the behavior of the system in the vicinity of the critical point P_c, E_c, we showed that power law distributions arise in the break-up of shells due to an underlying phase transition between the damaged and fragmented states, which proved to be abrupt for explosion, and continuous for impact.

The experimental study was done on hen egg-shells and hollow glass and plastic spheres as well. The break-up of the shells were studied under two different loading conditions, *i.e.* explosion caused by a combustible mixture and impact with the hard ground were considered. As the main outcome of the experiments, the mass distribution of fragments proved to be a power law in both loading cases for small fragment sizes. However, qualitative differences were obtained in the limit of large fragments for the shape of the cut-off. High speed pictures give insight in the fragmentation mechanisms. We demonstrated that numeric simulations in combination with simple experiments can give insight in the fragmentation process. We hope our work can help in interpreting and scaling statistical break-up models like Johnson et al. (2001) in future.

REFERENCES

J. A. Aström, B. L. Holian, and J. Timonen, *Phys. Rev. Lett.* **84**, 3061 (2000).

J. Åström and J. Timonen, *Phys. Rev. Lett.* **78**, 3677 (1997); J. Åström, M. Kellomäki and J. Timonen, *Phys. Rev. E* **55**, 4757 (1997).

W. Benz and E. Asphaug, *Icarus* **107**, 98 (1994).

A. Fujiwara and A. Tsukamoto, *Icarus* **44**, 142 (1980).

H. Inaoka, E. Toyosawa, and H. Takayasu, *Phys. Rev. Lett.* **78**, 3455 (1997).

N.L. Johnson, et al., *Adv. Space Res.* **28** 1377 (2001).

T. Kadono, *Phys. Rev. Lett.* **78**, 1444 (1997).

F. Kun and H. J. Herrmann, *Phys. Rev. E* **59**, 2623 (1999); F. Kun and H. J. Herrmann, *Comput. Meth. Appl. Mech. Eng.* **138**, 3 (1996).

H. Klinkrad, et al., *Adv. Space Res.* **28** 1355 (2001).

M. Oswald, et al., *AIAA*-2004-5221 (2004).

A. V. Potapov, M. A. Hopkins and C. S. Campbell, *Int. J. of Mod. Phys.* **C 6**, 399 (1995).

S. Redner, in *Statistical Models for the Fracture of Disordered Media*, edited by H. J. Herrmann and S. Roux (North Holland, Amsterdam, 1990).

C. Thornton, K. K. Yin and M. J. Adams, *J. Phys. D Appl. Phys.* **29**, 424 (1996).

D. L. Turcotte, *J. of Geophys. Res.* **91 B2**, 1921 (1986).

F. Wittel, F. Kun, B.-H. Kröplin, and H. J. Herrmann, *Phys. Rev. Lett.* **93**, 035504 (2004); F. Wittel, F. Kun, B.-H. Kröplin, and H. J. Herrmann, *Phys. Rev. E***71**, 016108 (2005).